

Drag Coefficients of Inclined Hollow Cylinders: RANS versus LES

A Major Qualifying Project Report

Submitted to the Faculty of the
WORCESTER POLYTECHNIC INSTITUTE

in partial fulfillment of the requirements for the
Degree of Bachelor of Science
In Chemical Engineering

By

Ben Franzluebbers _____

Date: April 2013

Approved:

Dr. Anthony G. Dixon, Advisor

Abstract

The goal of this project was use LES and RANS (SST k- ω) CFD turbulence models to find the drag coefficient of a hollow cylinder at various inclinations and compare the results. The drag coefficients were evaluated for three angles relative to the flow (0° , 45° , and 90°) and three Reynolds numbers (1000, 5000, and 10000). The drag coefficients determined by LES and RANS agreed for the 0° and 90° inclined hollow cylinder. For the 45° inclined hollow cylinder the RANS model predicted drag coefficients about 0.2 lower the drag coefficients predicted by LES.

Executive Summary

The design of catalyst particles is an important topic in the chemical industry. Chemical products made using catalytic processes are worth \$900 billion a year and about 75% of all chemical and petroleum products by value (U.S. Climate Change Technology Program, 2005). The catalyst particles used for fixed bed reactors are an important part of this. Knowing properties of the catalyst particle such as the drag coefficient is necessary to understand how fluid flow will be affected by the packed bed. The particles are inclined at different angles in the reactor and can come in a wide variety of shapes meaning that understanding the effect of particle shape on drag coefficient has practical importance. The drag coefficient is also important in areas such as chemical blending, mineral processing, powder sintering, processing of large food particles, and pneumatic and hydraulic conveying of particles (Tran-Cong, Gay & Michaelides, 2004). Since it is not always practical to experimentally test the drag coefficient for every particle at every Reynolds number, Computational Fluid Dynamics (CFD) is a useful tool to easily find the drag coefficient for various inclinations and Reynolds numbers.

The goal of this project was to calculate the drag coefficient of a hollow cylinder at several different Reynolds numbers and inclinations obtained by using the SST k- ω model (a RANS model) and compare to the drag coefficient obtained using LES. This comparison would be used to determine whether it is necessary to use LES to find a hollow cylinder's drag coefficient or if steady RANS is sufficiently accurate for most purposes. For this purpose Gambit 2.4.6 was used to model a hollow cylinder with a length of 1 inch, outer diameter of 1 inch, and inner diameter of 0.2868 inches. Then FLUENT 6.3.26 was used for the CFD simulations using both the SST k- ω model and LES for flow of air around a hollow cylinder at three Reynolds numbers (1000, 5000, and 10000) and three particle angles (0° , 45° , and 90°). The results were checked to ensure the solution was independent of both the domain size and the mesh coarseness. The results were validated by comparing CFD results for flow around a sphere with experimental data on the drag coefficient of spheres.

The results showed several trends. The SST k- ω model and the LES model both gave similar drag coefficients for the hollow cylinder angled at 0° or 90° with respect to the main flow direction but different drag coefficients for the 45° angled hollow cylinder. It would be necessary to use LES to estimate the drag coefficient of a hollow cylinder angled between 0° and 90° relative to the main flow. The values of the drag coefficient determined by CFD were found to differ from the values given by the correlation developed by Hölzer & Sommerfeld (2008). Two explanations for this were suggested. The 90° hollow cylinder was found to have a very similar velocity profile and drag coefficient as a 90° full cylinder. The correlation's predicted drag coefficient for a 90° full cylinder agreed more closely with the results found using CFD. Also, the correlation could be inaccurate for some of the angled hollow cylinders.

Table of Contents

| | |
|---|----|
| Abstract | 2 |
| Executive Summary..... | 3 |
| List of Figures | 5 |
| Introduction | 6 |
| Background..... | 8 |
| Drag coefficient | 8 |
| Drag Coefficient Dependence on Reynolds Number, Shape, and Orientation..... | 9 |
| Drag Coefficient Correlations..... | 13 |
| Computational Fluid Dynamics..... | 14 |
| RANS (SST k- ω)..... | 15 |
| LES | 16 |
| Methodology | 17 |
| Creating the Mesh..... | 17 |
| Running the CFD with SST k- ω Turbulence Model..... | 19 |
| Running the CFD with LES | 20 |
| Results | 21 |
| Comparisons between CFD Simulations and Experimental Data | 21 |
| Hollow Cylinder Comparisons | 22 |
| Comparison between k- ω and LES | 29 |
| Checking Domain and Mesh..... | 30 |
| Conclusion and Recommendations..... | 32 |
| References | 33 |

List of Figures

| | |
|---|----|
| Figure 1. Different Catalyst Shapes (Afandizadeh & Foumeny, 2001)..... | 8 |
| Figure 2. Example Catalyst Particles (Eigenberger & Ruppel, 2012)..... | 9 |
| Figure 3. Cylinder Drag Coefficients as a Function of Reynolds Number (Hoerner, 1958) | 10 |
| Figure 4. Flow Patterns Around a Cylinder (http://www.grc.nasa.gov/WWW/k-12/airplane/dragsphere.html) | 10 |
| Figure 5. Experimental Drag Coefficients of Different Shapes (Hölzer & Sommerfeld, 2008)..... | 11 |
| Figure 6. Flow Around Splitter, Cylinder, and Streamlined Body (Hoerner, 1958)..... | 12 |
| Figure 7. Tube Packed with Steam Reforming Catalyst (Stitt, 2005) | 13 |
| Figure 8. 0°, 45°, and 90° Angled Hollow Cylinder | 17 |
| Figure 9. ZY Side View of Solution Geometry | 18 |
| Figure 10. 45° Hollow Cylinder Mesh..... | 19 |
| Figure 11. Comparison between k- ω Simulation, Correlation, and Experimental Drag Coefficients for Flow around Sphere (Roos & Willmarth, 1971), (Preukschat, 1962)..... | 21 |
| Figure 12. 0° Hollow Cylinder, Comparison of Correlation, k- ω , and LES..... | 22 |
| Figure 13. 45° Hollow Cylinder, Comparison of Correlation, k- ω , and LES..... | 22 |
| Figure 14. 90° Hollow Cylinder, Comparison of Correlation, k- ω , and LES..... | 23 |
| Figure 15. Re=1000, Comparison of Correlation, k- ω , and LES | 24 |
| Figure 16. Re=5000, Comparison of Correlation, k- ω , and LES | 24 |
| Figure 17. Re=10000, Comparison of Correlation, k- ω , and LES | 25 |
| Figure 18. Velocity Vectors (m/s), 0° Hollow Cylinder, LES, Re=5000 | 25 |
| Figure 19. Velocity Vectors (m/s), 45° Hollow Cylinder, LES, Re=5000 | 26 |
| Figure 20. Velocity Vectors (m/s), 90° Hollow Cylinder, LES, Re=5000 | 26 |
| Figure 21. 90° Hollow and Full Cylinder, Comparison of Correlation, k- ω , and LES | 27 |
| Figure 22. Velocity Vectors (m/s), 90° Full Cylinder, k- ω , Re=5000..... | 28 |
| Figure 23. Velocity Vectors (m/s), 90° Hollow Cylinder, k- ω , Re=5000 | 28 |
| Figure 24. Velocity Contours (m/s), k- ω , 45°, Re=5000..... | 29 |
| Figure 25. Velocity Contours (m/s), LES, 45°, Re=5000 | 30 |
| Figure 26. Static Pressure (Pa), k- ω , 45°, Re=1000 | 31 |

Introduction

The drag coefficient of a particle in a flow is in many cases a useful parameter to know, with applications in chemical and other industries. The drag coefficient is important for the design of particles used in fixed and fluidized bed reactors, processing of large food particles, and pneumatic and hydraulic conveying of particles (Chhabra, Agarwal & Sinha, 1999). It is also essential for determining the settling behavior of solids in liquids which has uses in “chemical blending, mineral processing, powder sintering, manufacturing with phase change and solidification processes” (Tran-Cong, Gay & Michaelides, 2004). Because of this it is important to have ways to determine the drag coefficient of a particle.

The use of catalyst particles is particularly important. Chemical products made using catalytic processes are worth \$900 billion a year and about 75% of all chemical and petroleum products by value (U.S. Climate Change Technology Program, 2005). One of the most important components for this is fixed bed reactors. Fixed bed reactors contain a “bed” of solid catalyst pellets. The gas or liquid phase feed flows through the bed and is catalyzed by the particles. Since the bed is randomly packed the catalyst particles are inclined at different angles in the reactor. This is one reason why knowing the effect of particle angle on the drag can be useful. Also, catalyst particles come in a wide variety of shapes meaning that understanding the effect of particle shape on drag coefficient has practical importance.

Typically the drag coefficient would be found by performing an experiment which measures the drag force on a particle and uses that to calculate the drag coefficient. If an experiment cannot be performed or if an experiment is impractical then other methods are required. Analytical solutions have been found for the drag coefficient of spheres at low Reynolds numbers (Hölzer & Sommerfeld, 2008). For other situations, many correlations have been developed to estimate the value of a particle’s drag coefficient based on known parameters, usually the Reynolds number and some shape factor for the particle. For this project the correlation developed by Hölzer & Sommerfeld was used to estimate the drag coefficient of a hollow cylinder at combinations of several different angles and Reynolds numbers. The correlation matches experimental data for cylinders at different Reynolds numbers with an acceptable range of error. It calculates the drag coefficient using the Reynolds number of the flow as well as the sphericity and crosswise sphericity of the particle.

Running experiments to determine a particle’s drag coefficient can be impractical in many situations due to the time and money they require. On the other hand, relatively simple correlations for the drag coefficient such as the one developed by Hölzer & Sommerfeld can have sizable error compared to experimental values. One way of finding relatively accurate values of the drag without taking too much time is with computational fluid dynamics (CFD) programs. CFD generally involves finding a numerical solution to the Navier-Stokes equations describing the fluid flow (Priyadarshini, 2012). For this project two CFD techniques to model turbulence were used: the SST k- ω model using steady state Reynolds averaged Navier-Stokes (RANS) equations and unsteady state Large Eddy Simulation (LES). The steady RANS is much quicker to calculate than LES, but it fails to take into account the unsteady nature of the turbulent flow (Salim, Ong & Cheah, 2011).

The goal of this project was to compare the drag coefficient of a hollow cylinder at different inclinations obtained by using steady RANS with the drag coefficient obtained using unsteady LES. From this it could be determined whether it is necessary to use LES to find a hollow cylinder's drag coefficient or if steady RANS is sufficiently accurate for most purposes. For this purpose the CFD program FLUENT 6.3.26 was used and simulations were done using both the k- ω model and LES for flow around a hollow cylinder at three Reynolds numbers (1000, 5000, and 10000) and three particle angles (0° , 45° , and 90°). Validation of results was done by comparing CFD results for a sphere with experimental data on the drag coefficient of spheres.

Background

Drag coefficient

When fluid flows around an object (or when an object travels through a fluid), the fluid causes a force that acts on the object in the direction of the flow which is called drag force. This force can be calculated using a drag coefficient, a dimensionless number that is determined experimentally. The following equation shows the relationship between drag force on a particle and the drag coefficient:

$$F_D = \frac{1}{2} * \rho * u^2 * C_D * A$$

where F_D is the drag force, ρ is the fluid density, u is the velocity of the fluid relative to the particle, C_D is the drag coefficient of the particle, and A is the reference area: the cross sectional area a volume equivalent sphere.

In the case where the particle Reynolds number is very low, Stokes' law (shown in the following equation) can be used to calculate the drag force without needing to know the drag coefficient.

$$F_D = 6 * \pi * \mu * r * u_s$$

where μ is the dynamic viscosity of the fluid, r is the radius of the particle, and u_s is the settling (or terminal) velocity of the particle. Stokes' law can be very useful for determining the settling characteristics of a particle or particles in a fluid, but it does have limitations. It only applies to flows with low Reynolds numbers where turbulence is not an issue and it is designed for spheres and other similarly shaped particles. Many situations involve turbulent flow around non-spherical particles, and it can be important to know the relevant particle drag coefficient in those cases. For example, fluidized bed reactors are often filled with catalyst particles with unusual shapes, some of which are shown in Figure 1 and 2 below. The drag coefficient is useful to know for those sorts of practical applications.

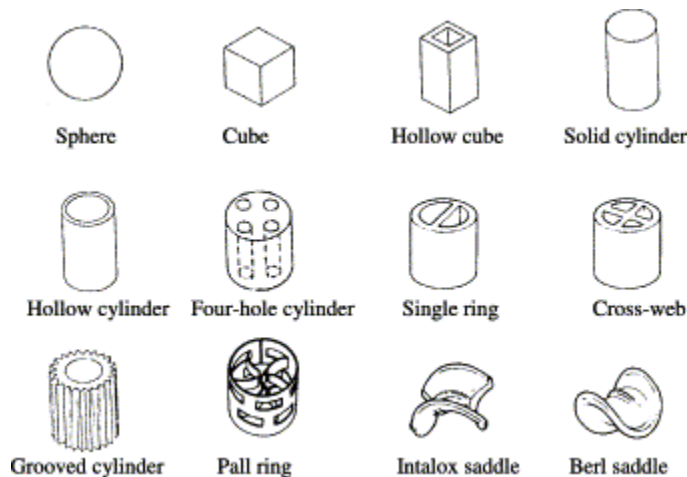


Figure 1. Different Catalyst Shapes (Afandizadeh & Foumeny, 2001)



Figure 2. Example Catalyst Particles (Eigenberger & Ruppel, 2012)

Figure 2 shows a picture of several different types of catalyst particles, including some hollow cylinders.

There is a lot of experimental data on the drag coefficient of common shapes such as spheres, but not much experimental data on hollow cylinders. For this reason spheres were chosen to validate this project's procedures. There is some experimental data on the drag coefficient of full cylinders with equal length and diameter, but these deal mainly with low Reynolds number flows (for example, Michaelides (2006) shows drag coefficients for Reynolds numbers from 0.1 to 400). The closest shape to a hollow cylinder which has plenty of experimentally measured drag coefficients is a sphere.

Drag Coefficient Dependence on Reynolds Number, Shape, and Orientation

As previously mentioned, the Reynolds number of fluid flow around a particle has an effect on the value of the drag coefficient. The particle Reynolds number is defined as the fluid velocity relative to the particle (u) times the characteristic dimension (d) of the particle (which is the diameter of the volume equivalent sphere) divided by the kinematic viscosity (ν) of the fluid:

$$Re = \frac{u * d}{\nu}$$

The typical relationship between particle Reynolds number and the experimental drag coefficients of cylinders is demonstrated in Figure 3. In general the drag coefficient decreases as the Reynolds number increases from low numbers up to around 10. This range is known as the Stokes region. At Reynolds numbers equal to 1000 the drag coefficient begins to level off and stays approximately constant. This range is known as the Newton region. When the Reynolds number increases between 10^5 and 10^6 the drag coefficient rapidly decreases before increasing a small amount.

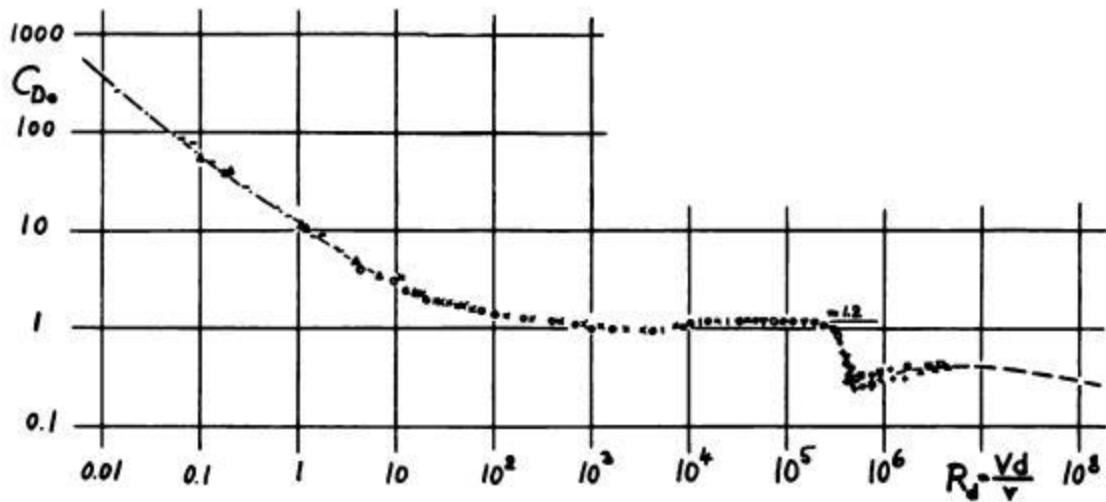


Figure 3. Cylinder Drag Coefficients as a Function of Reynolds Number (Hoerner, 1958)

The drag coefficient decreases linearly at low Reynolds numbers and then essentially levels off at higher numbers. This means that at low Reynolds numbers drag force increases linearly with velocity (as Stokes' law predicts) but at high Reynolds numbers drag force increases proportionally with velocity squared. Figure 4 shown below helps to indicate the reasons for the particular shape of the drag coefficient curve.

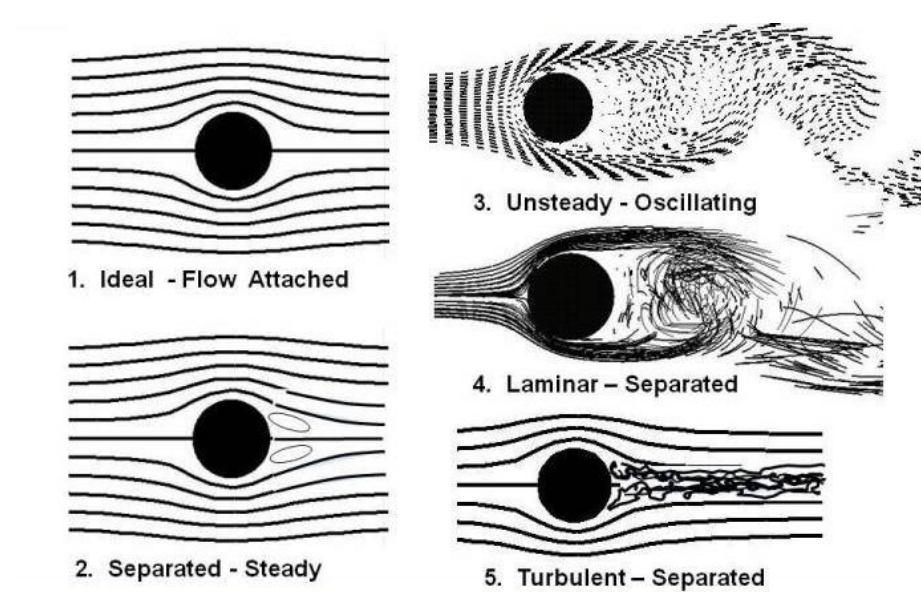


Figure 4. Flow Patterns Around a Cylinder (<http://www.grc.nasa.gov/WWW/k-12/airplane/dragSphere.html>)

Figure 4 shows the flow pattern of fluid around a cylinder. At low Reynolds number (drawing 2), there is steady state flow around the cylinder with two vortices right behind the cylinder which are the reason for the large drag coefficients. Drawing 3 shows what happens when the Reynolds number increases enough to transition into turbulence. The flow causes unsteady but periodic eddies behind the cylinder

with the wide wake causing much of the drag. Drawing 4 shows what happens when the flow gets to the region where the drag coefficient levels off. The boundary layer around the cylinder is laminar and the wake is no longer repeating but instead is extremely chaotic. Finally, Drawing 5 shows the flow pattern when the Reynolds number is high enough that the boundary layer between the fluid flow and the cylinder becomes turbulent and the separation point moves downstream. The downstream separation point is the cause of the sharp drop in the drag coefficient.

In addition to Reynolds number, a particle's shape also has an effect on the drag coefficient. Figure 5 shows the experimental drag coefficients for a number of shapes over a wide range of Reynolds numbers.

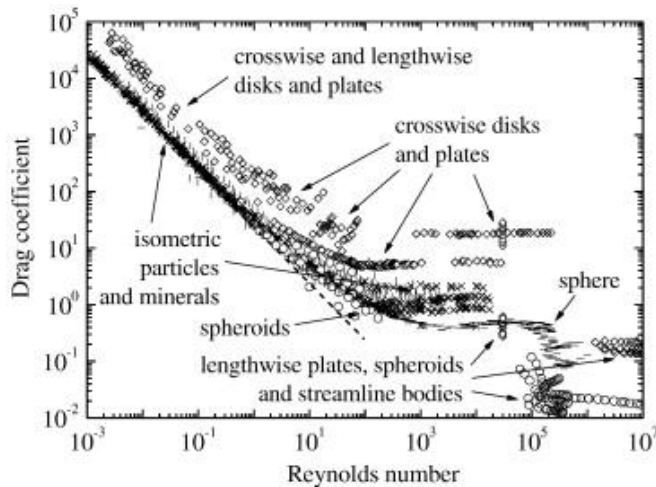


Figure 5. Experimental Drag Coefficients of Different Shapes (Hölzer & Sommerfeld, 2008)

Figure 5 shows what the drag coefficient values tend to be for different groups of particle shapes. Generally particles which are streamlined (designed to have low drag), spheres or spheroids, and lengthwise plates (plates with their longest side pointing in the same direction as the flow) have lowest drag coefficients. They all tend to have similar drag coefficients at the low Reynolds numbers but they separate a little at high Reynolds numbers. The next lowest drag coefficients tend to belong to particles which are isometric (having sides of equal length like a cube). They have drag coefficients similar to the spheres, lengthwise plates, spheroids, and streamline bodies at low Reynolds numbers, but their drag coefficients are larger at higher Reynolds numbers. The class of particles with the largest drag coefficients is the crosswise disks and plates (largest cross sectional area facing in the direction of the flow). These particles consistently have higher drag coefficients across the entire range of Reynolds numbers.

Differences in values of the drag coefficient between different shapes can largely be explained by the different flow patterns that result from different shapes and their orientations. Figure 6 below shows the flow pattern around several different particle shapes.

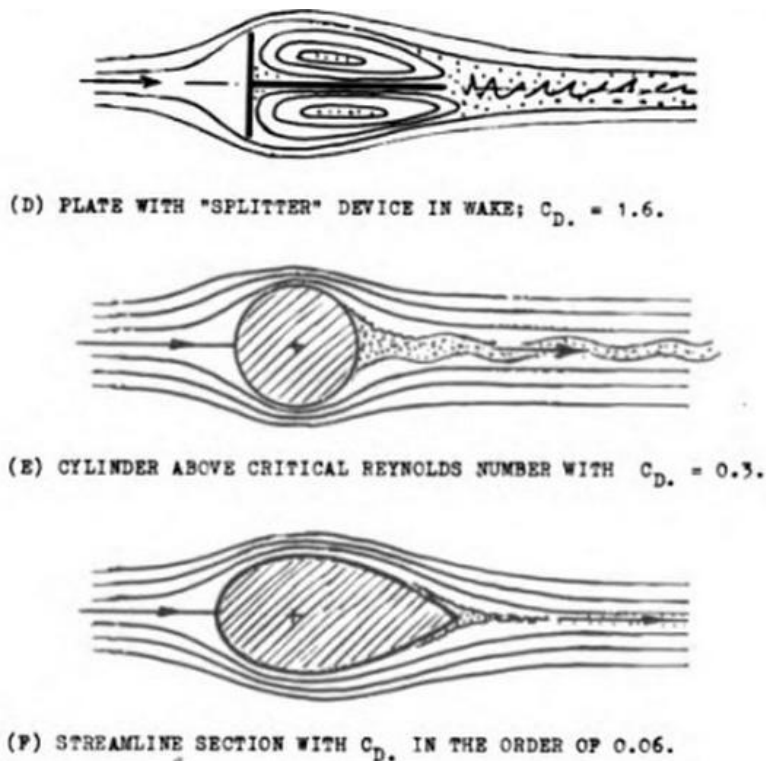


Figure 6. Flow Around Splitter, Cylinder, and Streamlined Body (Hoerner, 1958)

Drawing D shows flow around a crosswise plate with a splitter behind it. The sudden large flat area forces rapid change in flow direction and the splitter separates the wake behind the plate into two very large vortices. The result of these large vortices is a very high drag coefficient. Drawing E shows crosswise flow around an infinitely long cylinder. The more gradual change in flow direction around the circular cylinder results in a smaller turbulent wake. The cylinder has a lower drag coefficient than the crosswise plate. The shape with the lowest drag coefficient is the streamline section shown in drawing F. It is shaped and angled so that the change in the flow direction is even smaller than the change around the cylinder and as a result it has a small, almost nonexistent, wake trailing behind it which is the reason it has such a low drag coefficient.

It is clear that the orientation of a particle with respect to the flow direction can have an effect on the particle's drag coefficient. Experimental data shows that lengthwise plates have some very low drag coefficients, while crosswise plates have some of the highest drag coefficients. Crosswise plates have large flat areas facing the fluid direction which leads to the large wakes and consequently large drag coefficients. Lengthwise plates act more like the streamlined section, only requiring slight displacements for the fluid flow to go around them. This leads to the low drag coefficients that lengthwise plates have. Less extreme differences in drag coefficient can be caused by different shapes pointing at different angles relative to the flow direction.

The dependence of drag coefficient on particle orientation can be important since in many cases a particle may not be fixed in one direction while flow goes around it. Some particles, such as cylinders with equal length and diameter will not fall in one orientation but instead spin in different directions

(Christiansen & Barker, 1965). Even if particles are fixed like in a packed bed reactor, the individual particles can be at different orientations. Figure 7 shows an example of a steam reforming packed bed reactor with the catalyst particles packed at a variety of different angles.



Figure 7. Tube Packed with Steam Reforming Catalyst (Stitt, 2005)

Drag Coefficient Correlations

Drag coefficients of particles can be difficult to determine experimentally. Many drag coefficients are found by either determining settling velocities of particles at low Reynolds numbers or testing particles in wind tunnels at high Reynolds numbers (Hölzer & Sommerfeld, 2008). Since determining drag coefficients for particles can sometimes be difficult or impractical, many empirical correlations have been developed to estimate the values without requiring any experiments. These correlations are generally based off more well established data for sphere drag coefficients, with corrections added in to account for different shapes and orientations as well as different Reynolds numbers.

This project focuses on the correlation developed by Hölzer & Sommerfeld (2008). The correlation integrates the research used to create several earlier correlations. Hölzer & Sommerfeld combined a correlation applying to low Reynolds numbers developed by Leith (1987), modified correlation given by Ganser (1993) that covers drag coefficients at high Reynolds numbers, and an additional term added by Tran-Cong, Gay & Michaelides (2004) to more accurately reflect experimental data. In addition, Hölzer & Sommerfeld modified the terms to better fit the data. The correlation they developed was this:

$$C_D = \frac{8}{Re * \sqrt{\Phi_{\parallel}}} + \frac{16}{Re * \sqrt{\Phi}} + \frac{3}{\Phi^{3/4} * \sqrt{Re}} + 0.42 * 10^{0.4 * (-\log(\Phi))^{0.2}} * \frac{1}{\Phi_{\perp}}$$

where Φ_{\parallel} is lengthwise sphericity, Φ is sphericity, and Φ_{\perp} is cross sectional sphericity.

Sphericity is the ratio of the surface area of a sphere with the same volume as the particle to the surface area of the particle, which becomes the following equation:

$$\Phi = \frac{\pi^{1/3} * (6 * V)^{2/3}}{A}$$

where V is particle volume and A is the particle surface area. The sphericity is used to correct for the shape of the particle.

Cross sectional sphericity is similar; it is the ratio of the cross sectional area of a sphere with the same volume as the particle to the projected cross sectional area of the particle perpendicular to the flow direction, which becomes the equation:

$$\Phi_{\perp} = \frac{\pi^{1/3} * (\frac{3}{4} * V)^{2/3}}{A_{\perp}}$$

The cross sectional sphericity for a given particle can differ depending on the inclination. The correlation uses it to correct for the differences in drag coefficient for particles at different angles relative to the direction of the main flow.

Lengthwise sphericity is ratio of the cross sectional area of a sphere with the same volume as the particle to the average of the longitudinal projected cross sectional area of the particle perpendicular to the flow direction. It is usually more difficult to calculate since it must be averaged over a range of different cross sectional areas determined by the particle orientation.

The reason this correlation was chosen was because it is relatively easy to use and has the best fit with experimental data. Hölzer & Sommerfeld calculated that the correlation had a 14.1% mean deviation from all available experimental data, with cuboids and cylinders having a 29% mean deviation. This is as accurate as drag correlations get for non-spherical shapes.

Computational Fluid Dynamics

Computational Fluid Dynamics (CFD) involves the use of computers to find numerical solutions to complex fluid dynamics problems. The Navier-Stokes equations are complex differential equations that have resisted easy solutions. CFD takes advantage of a computer's ability to perform fast calculations to find numerical solutions to these equations. CFD can be much more practical than performing experiments in a wind tunnel to determine fluid flow behavior. One important aspect to CFD is that it requires good input and modeling, or else all the fast calculating will be wasted since the program will return bad output.

The first step to solving a CFD problem is to define the relevant geometry. This can be done using a computer modeling software. Next, the geometry has to be divided into a mesh with a finite number of volumes that the geometry contains. After that the physical modeling and boundary conditions must be defined and the equations governing fluid flow must be chosen.

CFD generally involves finding numerical solutions to the Navier-Stokes equations. The user's guide to FLUENT, a CFD program, gives the following equation:

$$\frac{\partial(\rho * u)}{\partial t} + \nabla \cdot (\rho * u * u) = -\nabla * P + \nabla \cdot \tau + \rho * g + F$$

where ρ is the fluid density, t is time, ∇ is the del operator, u is the flow velocity, P is the pressure, τ is the stress tensor, g is the acceleration due to gravity, and F is any other body force acting on the model.

The other key equation to solve is the mass continuity equation, which the FLUENT user's guide defines as:

$$\frac{\partial \rho}{\partial t} + \nabla \cdot (\rho * u) = S_m$$

where S_m is mass added from a second phase, equal to zero for this project.

The process of solving these equations without making other simplifying assumptions is called Direct Numerical Simulation (DNS). Since it does not involve making big assumptions it can be very accurate, but it has downsides. The big issue is that DNS is extremely computer resource intensive and as a result is slow and not practical to use in many cases. It is only possible at low Reynolds numbers when turbulence is not an issue and the geometry is not very complex. In most cases simplifying assumptions must be made which allow for easier solutions, while still accurately modeling what goes on in actual fluid flow.

RANS (SST k- ω)

One common method for making the Navier-Stokes equations easier to solve is with Reynolds averaged Navier-Stokes (RANS). It involves first finding averaged values for the fluid velocity, pressure, and density (Fröhlich & von Terzi, 2008). These values are then used instead of their instantaneous values in the Navier-Stokes equations. Doing this necessitates the inclusion of Reynolds stresses in the equation to model the turbulence. To achieve this it is common to use the Boussinesq hypothesis, which says that these stresses can be estimated as being proportional to the mean strain rate (Ehrhard, Khatib, Winkler, Kunz, Moussiopoulos & Ernst, 2000). This hypothesis is reasonable for modeling simple turbulence such as boundary layer turbulence. RANS requires much less computing resources than DNS because of these simplifications.

One RANS model that uses the Boussinesq hypothesis is the k- ω model. It models eddy viscosity based on two variables, k for turbulent kinetic energy and ω for specific dissipation. Together with the governing equations, they model the turbulence.

One variation of the k- ω model is the Shear Stress Transport (SST) formulation. Walls are the main source for turbulence in a flow. Because of this it is important for the turbulence model to account for the area around walls. The SST k- ω model achieves this by using a zonal two layer model. It uses different models for different regions in the flow. Near the walls the k- ω model is more accurate so it is used, while in the free stream away from the wall the k- ϵ model is less sensitive to boundary condition turbulence issues so that is used (Menter, Kuntz, & Langtry, 2003). One important requirement for the k- ω model is that mesh around the wall must be very pristine so that the y^+ for cells around the wall should be approximately 1 (Fluent, 2006). y^+ is a dimensionless measure of distance from a wall and is defined as:

$$y^+ = \frac{u_\tau * y}{\nu}$$

Where y is the distance from the nearest wall, u_τ is the frictional velocity, and ν is the kinematic viscosity of the fluid.

LES

Large Eddy Simulation (LES) is another method used to simplify the Navier-Stokes equations by modeling turbulence. When there is turbulence in the flow there are eddies, swirling caused by flow past an object, which can greatly vary in terms of size. Large eddies can be difficult to model since they are affected by the direction of the flow, the history of the flow, the boundary conditions, and flow configuration. LES involves filtering the Navier-Stokes equations so that smaller eddies can be modeled instead of being directly solved while larger and harder to model eddies are resolved.

LES can account for the unsteady nature of turbulent flow better than RANS. LES models only small eddies and solves the transport equations for larger eddies, while RANS models all levels of turbulence. Because of this LES is more computationally expensive to run than RANS, but can potentially be more accurate. Still, it is much cheaper than DNS for situations with a high Reynolds number or a complex geometry.

Methodology

The drag coefficient correlation developed by Hölzer & Sommerfeld (2008) was used to calculate expected values for the drag coefficient of the angled cylinders at different Reynolds numbers. These values were compared with the results of the CFD simulations.

For this project Gambit 2.4.6 was used to create and mesh the geometry of the particle and Fluent 6.3.26 was used to simulate the fluid flow around the particle. The hollow cylinder had a length and outer diameter equal to 1 inch and an inner diameter equal to 0.2868 inches at the center.

Creating the Mesh

The first step was to use CFD to find the drag coefficient of spheres and then compare that information with experimental data from the literature to confirm that CFD was applicable for the project. The sphere was created with a 1 inch diameter. The meshes for the hollow cylinder were created at the same time. Three different angles were chosen for the particle: 0° , 45° , and 90° shown below in Figure 8. These angles were chosen to study the effect of very different angles on the drag coefficient. Gambit was used to model the geometry.

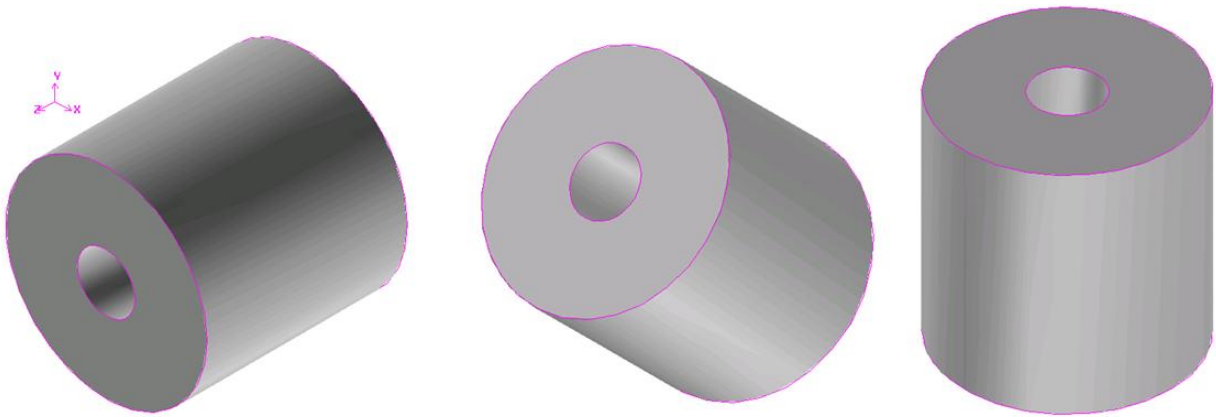


Figure 8. 0° , 45° , and 90° Angled Hollow Cylinder

Figure 8 shows the different angled cylinders from an isometric perspective. The flow goes directly into the circular face of the 0° cylinder on Figure 8's left. The flow goes around the curved outside of the 90° cylinder on Figure 8's right. The 45° cylinder is in between the two extremes.

To start creating the geometry a cylinder with length and diameter equal to one inch was created and centered around the z-axis. A cylinder with length equal to one inch and a diameter of 0.2868 inches was created and centered around the z-axis. This second cylinder was subtracted from the first to leave a single hollow cylinder. For the case of the 45° and 90° cylinders, the cylinder was rotated by the appropriate angle. Next, a "brick" with width of 15 inches, depth of 15 inches, and a height of 20 inches was created around the cylinder. These dimensions were chosen to allow plenty of room for flow around the particle, and most importantly to leave plenty of room for the turbulent wake. Another mesh with width of 20 inches, depth of 20 inches, and a height of 25 inches was created to compare

with the original mesh. This was done to ensure that the solution was independent of the dimensions of the mesh and that there was enough room for the turbulence to not be significantly affected by the walls of the solution. The side view of the geometry for the 0° angled particle is shown in Figure 9. The flow traveled from the left to the right.

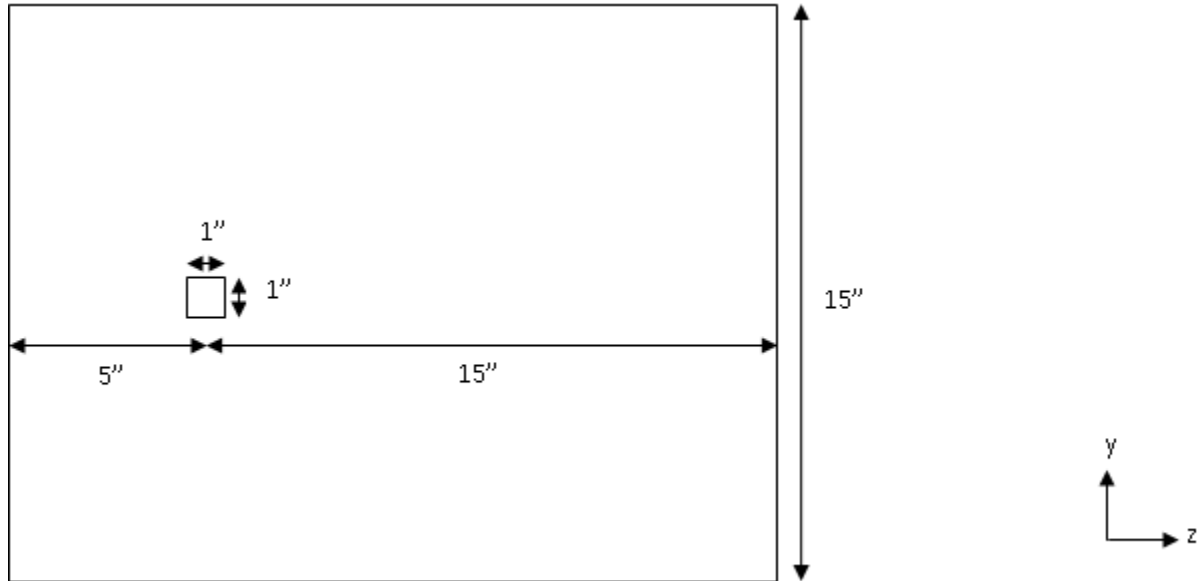


Figure 9. ZY Side View of Solution Geometry

After the geometry was defined it needed to be meshed so that it could be used in Fluent. Only the fluid portion of the geometry was meshed since diffusion through the solid particle was not modeled. A boundary layer mesh was necessary to account for the complex interactions around the surface of the particle. A boundary layer mesh between the particle and the fluid volume was created with a 0.003 inch first row, a growth factor of 1.1, and 10 rows total. This boundary layer mesh was chosen to following previous work. In addition, a sizing function between the particle and the fluid volume was created with a starting size of 0.05, a growth rate of 1.075, and a size limit of 0.5. Once this was done the geometry was meshed with the tetrahedral “Tgrid” method. Finally, the velocity inlet and pressure outlet were specified as well as the fluid zone and the mesh was exported to Fluent. Figure 10 below shows the finished mesh for the 45° cylinder. The 0° hollow cylinder mesh contained 199118 nodes, the 45° mesh contained 194864 nodes, and the 90° mesh contained 200390 nodes.

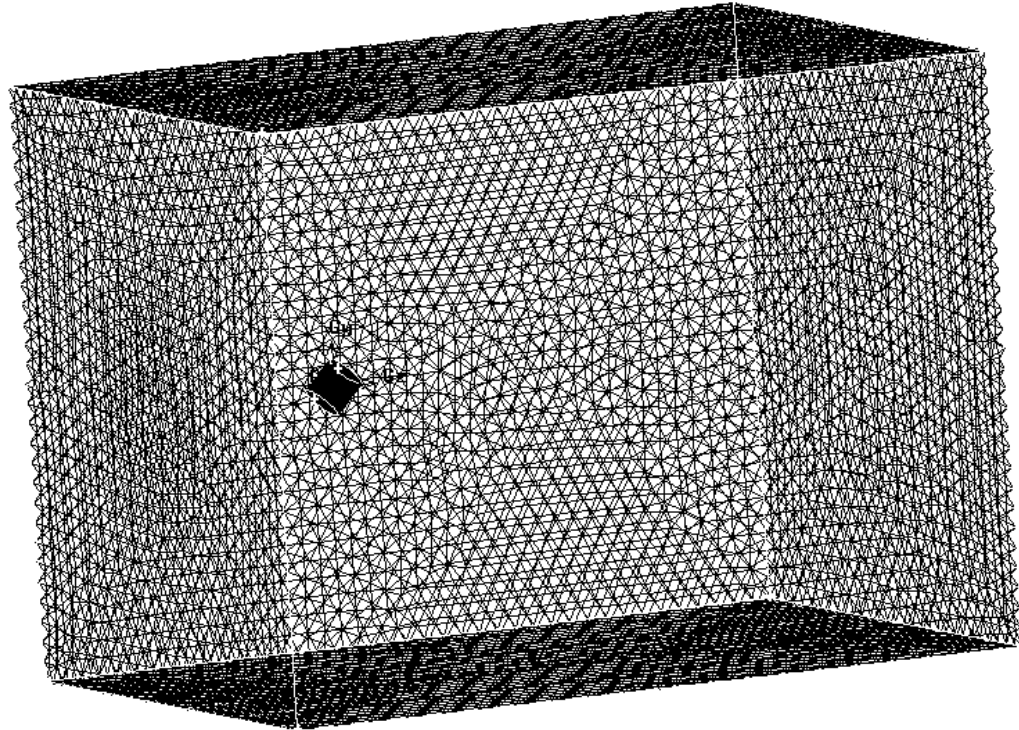


Figure 10. 45° Hollow Cylinder Mesh

The mesh for the sphere was set up in a similar manner. A sphere with a diameter of 1 inch was created and moved 5 inches into the long length of a 15 by 15 by 20 inch fluid zone. The boundary layer mesh between the sphere and the fluid was also applied to the sphere mesh. The remaining details involved in making the sphere mesh were the same as the steps used to create the hollow cylinder meshes. The sphere mesh contained 170443 nodes.

Running the CFD with SST $k-\omega$ Turbulence Model

Once the meshes were created the CFD simulations could be run. The meshes were imported into Fluent. First a grid check was performed to ensure that the mesh was working fine. The size was scaled to put everything in terms of meters instead of inches. Next the initial conditions for the simulation were set up with air being the fluid, temperature being 300 K, and pressure being 101325 Pa. Any specifications that are not mentioned in this section were assigned the default Fluent values. The 3D, steady state, pressure based solver was chosen and the energy equation was enabled. For the viscous model the $k-\omega$ model with shear stress transport (SST) and transitional flows was selected. Next the boundary conditions were set. Three Reynolds numbers were tested ($Re=1000$, 5000 , and 10000) to observe the effect of different Reynolds numbers on the drag coefficient for the different angles. At the inlet a constant velocity was set which corresponded with the Reynolds number that was being tested for air at standard conditions (inlet velocity= 0.466889 , 2.334443 , and 4.668887 m/s for the hollow cylinders). These velocities were calculated using the Reynolds number formula. At the outlet a gauge pressure was set to be 0 and at the walls the no-slip condition was specified.

The SIMPLE method for pressure-velocity coupling was chosen. 1st order discretization was used for momentum, turbulent kinetic energy, specific dissipation rate, and energy. The reference velocity for each Reynolds number was specified. The cross-sectional area of the volume equivalent sphere was calculated (0.000627 m²) and specified. The Fluent simulation was set up to use the drag force to calculate the drag coefficient. All the under-relaxation factors except for pressure were lowered by 0.2 to and the simulation was started. After some iterations (usually 15 to 30), when the calculated drag coefficient started to approach the expected value (around 1), the under-relaxation factors were changed back to their default values. This ensured that the Fluent simulation did not diverge too much when starting out, but still didn't take an unnecessarily long time to converge on a solution. The simulation was run until the drag coefficient was constant to 5 significant figures with each iteration. This typically took several thousand iterations.

Next the solutions were tested to make sure they were independent of both the domain size and the grid. The grid was adapted so that mesh would be more refined and the Fluent simulation was run again. Next 20 by 20 by 25 inch meshes were tested using the same SST k- ω conditions to check for domain independence.

The drag coefficients for the sphere were obtained in a similar manner. The velocities and cross sectional area were changed due to the different characteristic diameter (velocity=0.519379, 2.596896, and 5.193792 m/s, area= 0.000507 m²). The rest of the specifications were the same. The drag coefficients obtained for the spheres were compared to experimental data from the literature.

Running the CFD with LES

Once the data from the k- ω runs was obtained the runs using LES could be started. LES was used to find the drag coefficient for all three angled hollow cylinders at each Reynolds number. The instantaneous velocity field from the k- ω solution was used as the initialization. Smagorinsky-Lilly was used as the subgrid-scale model. Non-Iterative Time Advancement (NITA) with PISO was used to control the time step solutions. NITA was used to speed up the simulation while still preserving accuracy. The maximum number of corrections of the momentum equations was increased to 20 to allow the solver enough iterations to converge. For discretization the pressure was standard, the momentum used bounded central differencing, and the energy used first order upwind. Similarly to the k- ω runs, the under-relaxation factors for the pressure, momentum, and energy were decreased by 0.2. The time steps used were determined using the equation:

$$\Delta t = 0.02 * \frac{d}{u}$$

where u is the inlet velocity and d is the characteristic dimension. For example, when the Reynolds number is 1000 the time step was 0.00121047 s. Finally, Fluent was run using LES until the data was observed to be statistically stationary. The drag coefficient was not constant over time, but it went up and down in a regular manner. Then an average of the drag coefficients over several periods was recorded.

Hollow Cylinder Comparisons

Next the drag coefficients for the hollow cylinder were compared. The data from the k- ω and the LES simulations was compared with drag coefficients calculated from the correlation. Figure 12, 13, and 14 show the results for the 0°, 45°, and 90° angled hollow cylinders.

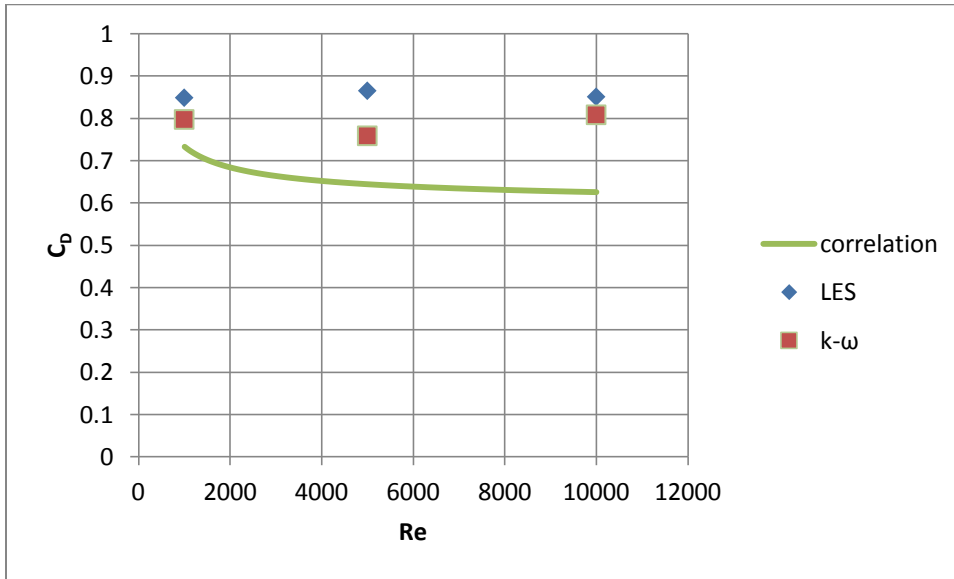


Figure 12. 0° Hollow Cylinder, Comparison of Correlation, k- ω , and LES

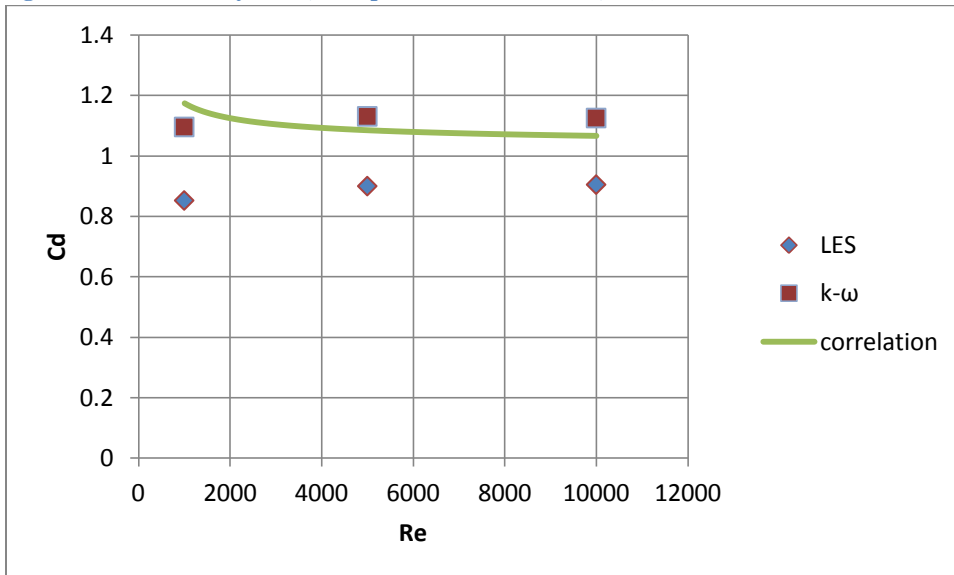


Figure 13. 45° Hollow Cylinder, Comparison of Correlation, k- ω , and LES

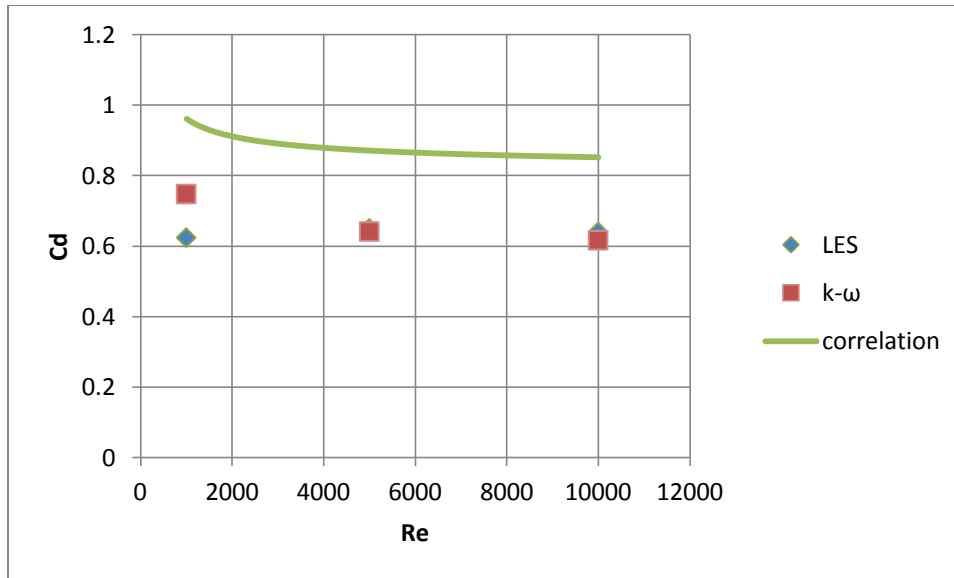


Figure 14. 90° Hollow Cylinder, Comparison of Correlation, k- ω , and LES

The general trend in the LES results is that the drag coefficients are mostly constant from Reynolds numbers from 1000 to 10000. This suggests that much like spheres and long cylinders, hollow cylinders at various inclinations have constant drag coefficients at Reynolds numbers from 1000 to 10000. Though the drag coefficient is mostly constant, there is a slight increase in value when the Reynolds number equals 5000. This is not unusual as shapes such as the sphere and the long cylinder have drag coefficients slightly increasing with increasing Reynolds numbers in the Newton region before eventually decreasing again (see Figure 3 and 5).

The drag coefficients computed using the SST k- ω model differ from the values given by the Hölzer & Sommerfeld (2008) developed correlation for some of the cases. For the 0° angled hollow cylinder the computed drag coefficients are higher than the values predicted by the correlation. For the 45° angled hollow cylinder the computed drag coefficients are approximately the same as the predicted values. For the 90° angled hollow cylinder the computed drag coefficients are lower than the predicted values. The results from the SST k- ω model go from overshooting the predicted values to undershooting as the angle increases.

Despite the similar trends in the LES, k- ω , and correlations drag coefficients, the actual values are off in many cases. The LES determined drag coefficient differs from the value given by the correlation by up to 35%. The differences for each Reynolds number can be seen in Figure 15, 16, and 17.

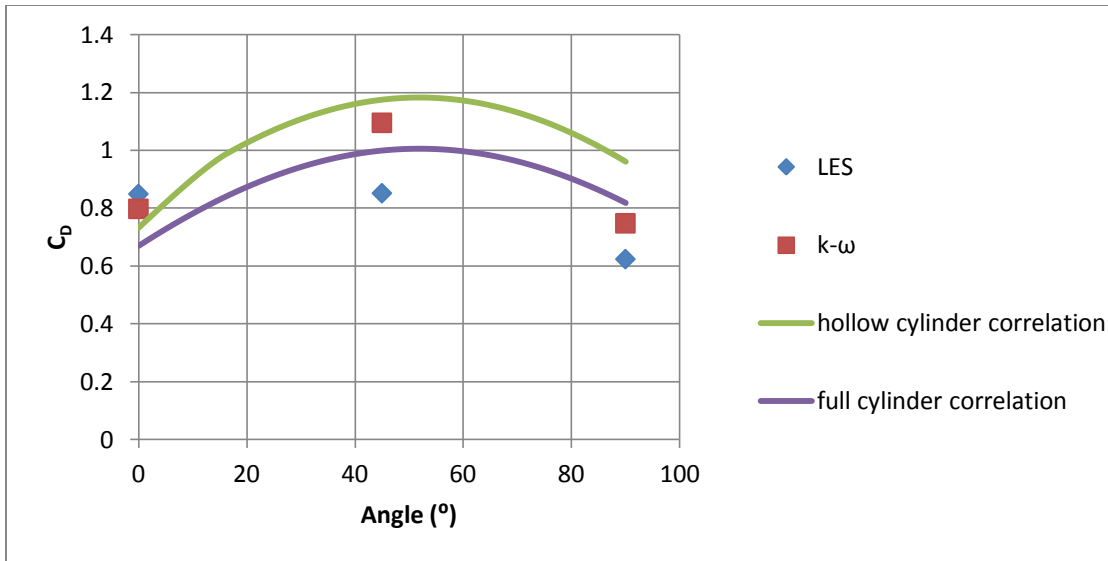


Figure 15. Re=1000, Comparison of Correlation, k- ω , and LES

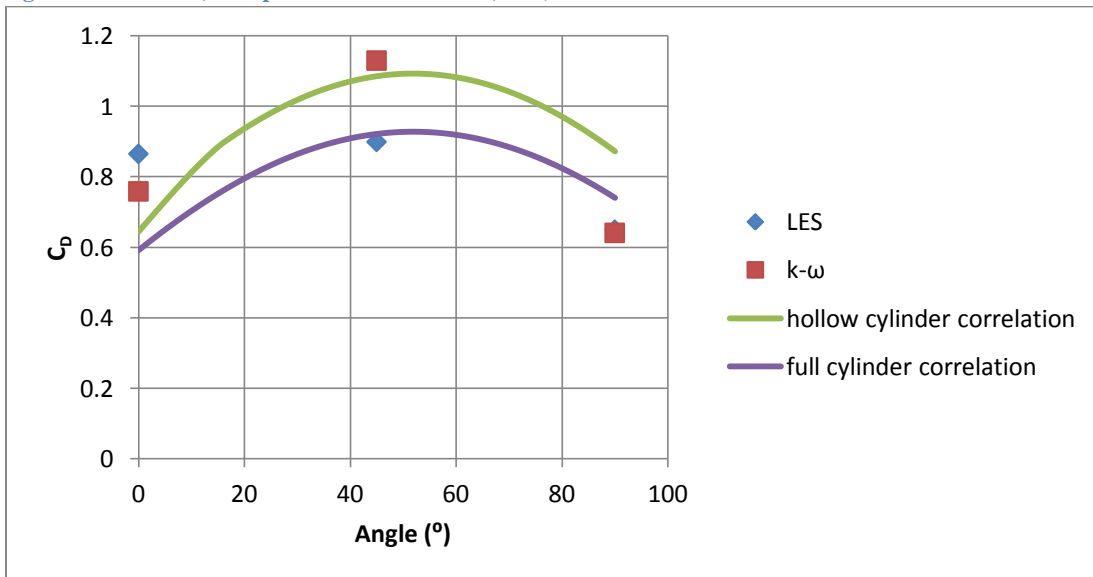


Figure 16. Re=5000, Comparison of Correlation, k- ω , and LES

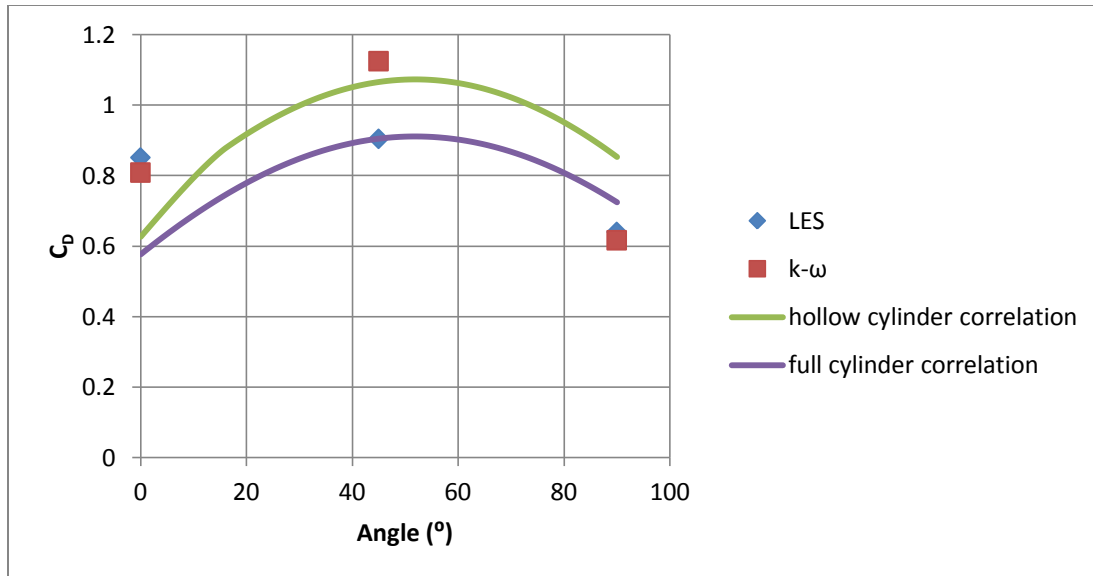


Figure 17. $Re=10000$, Comparison of Correlation, $k-\omega$, and LES

As Figure 15, 16 and 17 show, the drag coefficients determined using LES were over the predicted drag coefficients when the inclination angle was 0° but under the predicted value when the inclination angle was 45° or 90° . One possible reason for the low drag coefficients for the inclined hollow cylinders could be that at large angles the hollow cylinder behaves more like a full cylinder. While the 45° and 90° hollow cylinders have the same cross sectional area as the full cylinder, they do have lower sphericities. This is the reason why the correlation predicts higher drag coefficients for the hollow cylinder. Figure 18, 19 and 20 show a magnified side view of the velocity vectors going into and around the 0° , 45° , and 90° angled hollow cylinders.

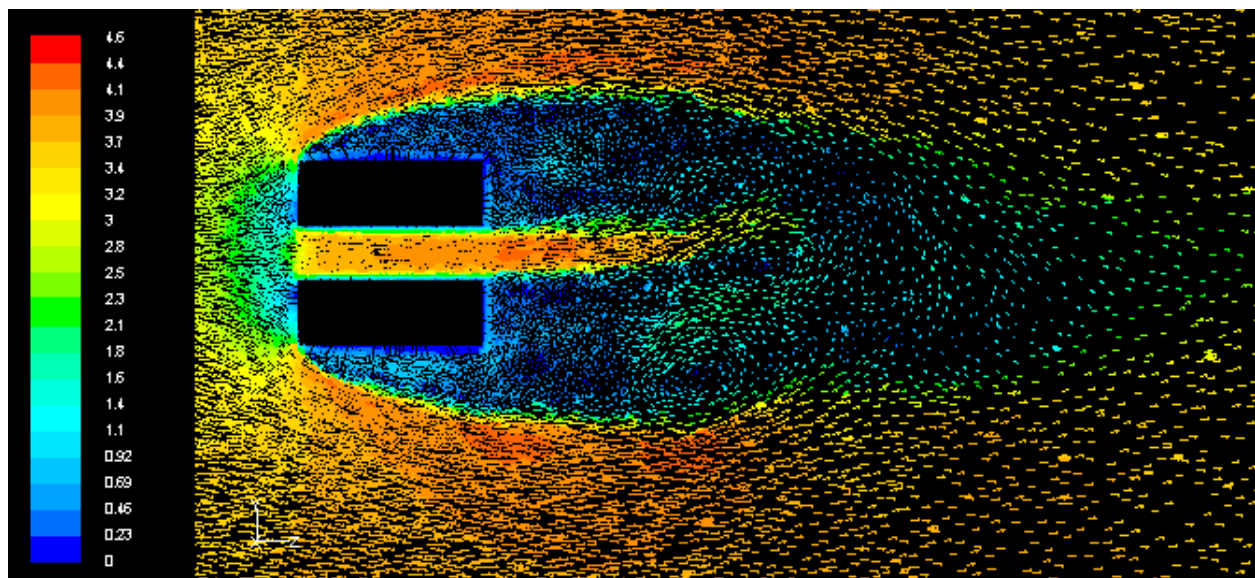


Figure 18. Velocity Vectors (m/s), 0° Hollow Cylinder, LES, $Re=5000$

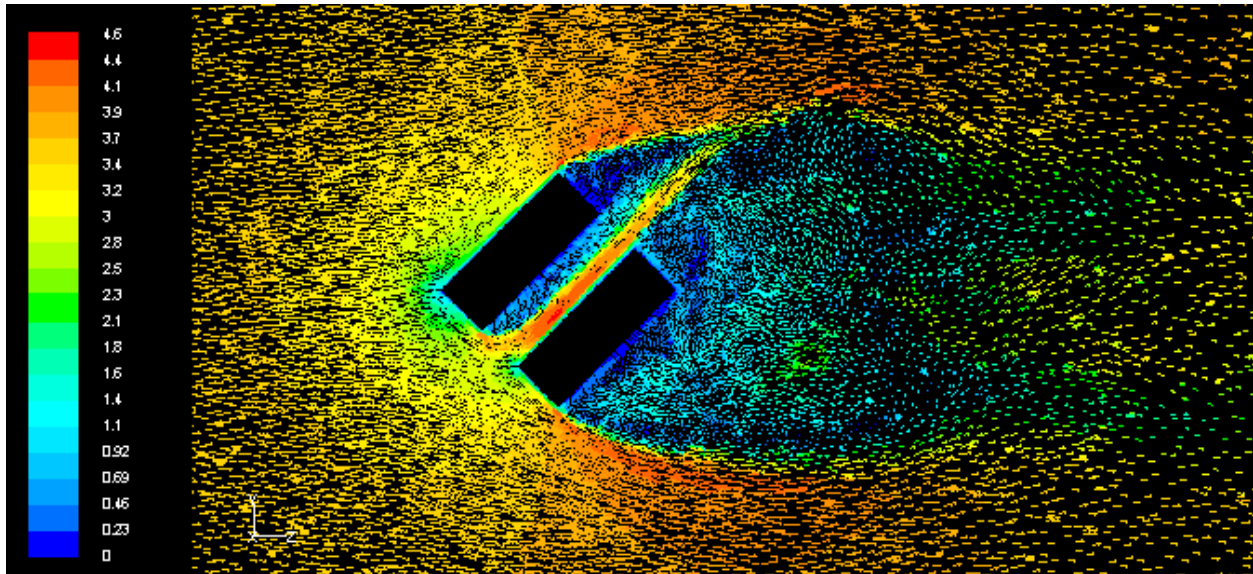


Figure 19. Velocity Vectors (m/s), 45° Hollow Cylinder, LES, Re=5000

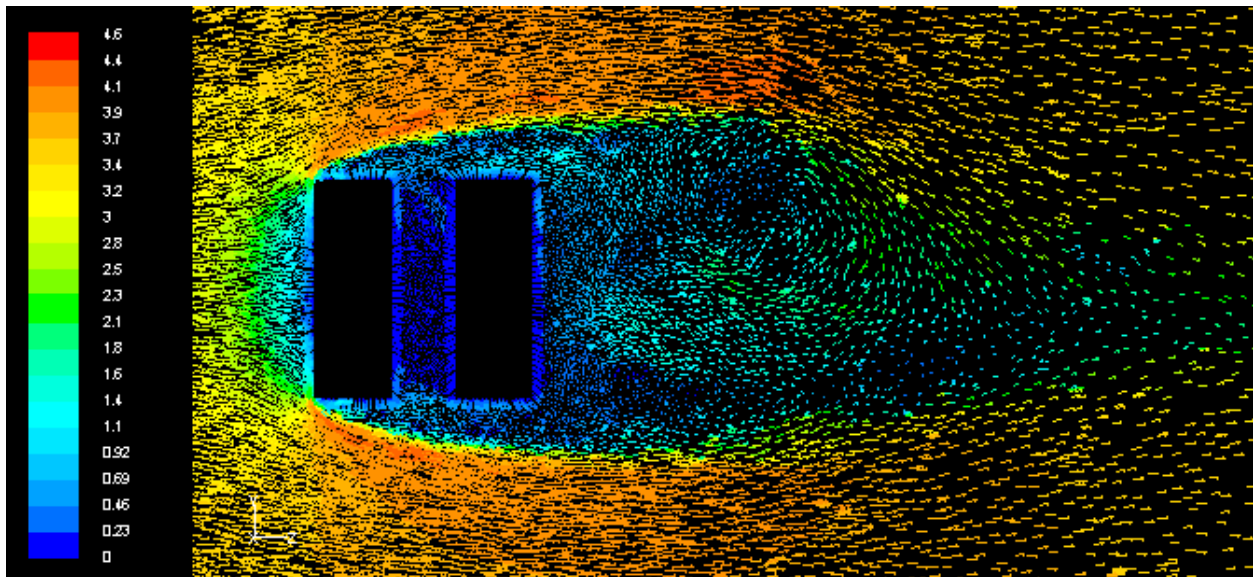


Figure 20. Velocity Vectors (m/s), 90° Hollow Cylinder, LES, Re=5000

As Figure 20 shows, there is not much velocity going through the 90° hollow cylinder's center. The velocity in the hole is near zero except at the edges. This could mean that the 90° hollow cylinder could be treated as a 90° full cylinder which would help explain why the LES determined drag coefficient is closer to the predicted full cylinder drag coefficient than to the predicted hollow cylinder drag coefficient.

The same effect might also partially explain why LES gave lower than expected drag coefficients for the 45° angled hollow cylinders. Figure 19 shows how the velocity field is somewhat in between the 0° and the 90° hollow cylinders. The 45° hollow cylinder does have some significant flow through its hole however, so the similarity to a full cylinder would probably not explain the entire difference between the LES determined drag coefficients and those calculated using the correlation. The 0° hollow cylinder, which behaves least like a full cylinder (due to the flow being able to flow straight through the hole) has

a drag coefficient which is closer to the result of the hollow cylinder correlation than the full cylinder correlation.

Figure 21 shows data for the 90° hollow and full cylinders. It shows the drag coefficients given by the correlation as well as data for the CFD determined drag coefficients of the hollow and full cylinders.

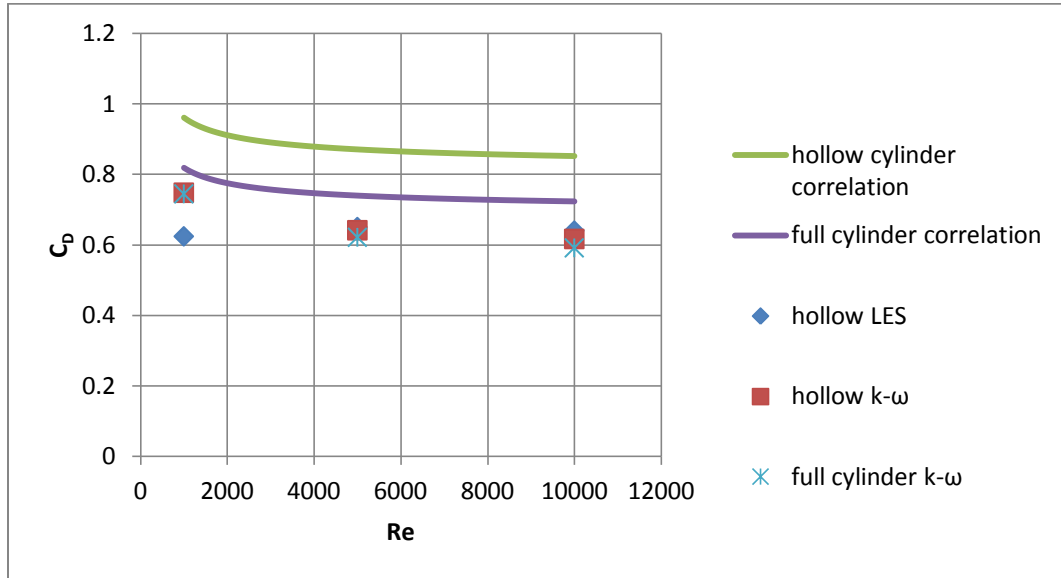


Figure 21. 90° Hollow and Full Cylinder, Comparison of Correlation, k- ω , and LES

The graph shows how the drag coefficients are very close for the hollow and full cylinder when the k- ω model is used. It also shows how the full cylinder correlation is a better fit to the CFD determined coefficients for both the full cylinder and the hollow cylinder.

Figure 22 and 23 show the velocity vectors around the 90° full cylinder and the 90° hollow cylinder calculated using the k- ω model.

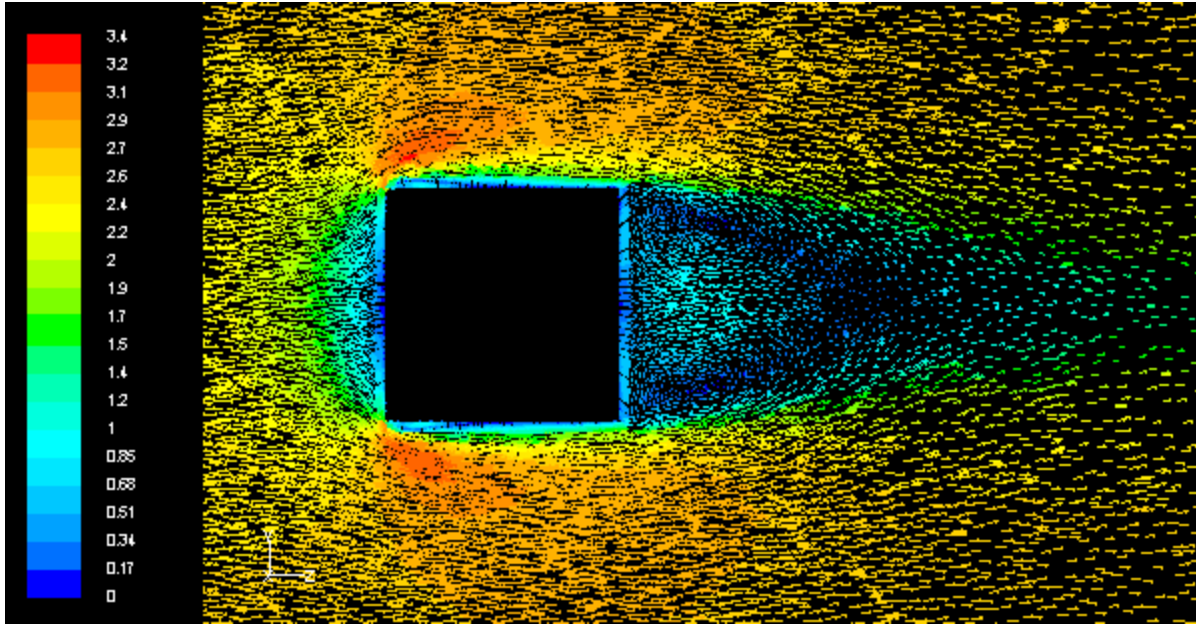


Figure 22. Velocity Vectors (m/s), 90° Full Cylinder, k- ω, Re=5000

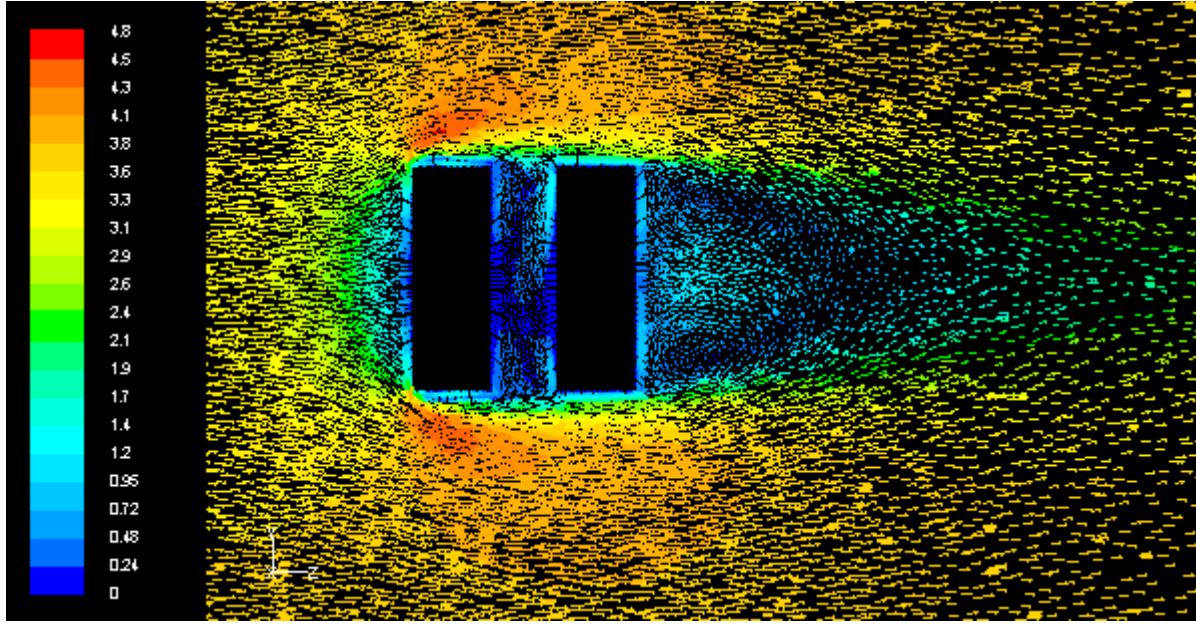


Figure 23. Velocity Vectors (m/s), 90° Hollow Cylinder, k- ω, Re=5000

Figure 22 and 23 give more evidence to the idea that the 90° hollow cylinder could be treated as a 90° full cylinder. The absolute values of velocity are slightly different due to the different entering fluid velocities, but when the ranges are appropriately scaled the plots of velocity vectors for both the full cylinder and hollow cylinder look very similar. The hole in the hollow cylinder does not seem to affect the velocity profile despite causing the hollow cylinder to have a lower sphericity than the full cylinder.

Another possible reason for the difference between the drag coefficient given by LES and the coefficient given by the correlation could be that the correlation could be inaccurate for hollow cylinders. The correlation is meant to be used for particles of any shape and orientation, not specifically hollow

cylinders. Also, the correlation was formed based off available experimental data that was largely different from this project's hollow cylinder angled at 0° , 45° , and 90° , and Reynolds numbers of 1000, 5000, and 10000. The correlation may be less accurate for these conditions.

Figure 15, 16, and 17 show that the angle of 45° consistently has the maximum drag coefficient. This is to be expected since the 45° angled hollow cylinder has the largest cross sectional area normal to the flow direction. As a result of this the 45° angled cylinder has the largest wake and the largest drag coefficient. The large wake can be seen in Figure 19 compared to Figure 18 and 20.

Comparison between k- ω and LES

Another goal of this project was to compare the drag coefficients obtained using LES with those obtained using k- ω . As Figure 12 and 14 show, both methods give reasonably similar drag coefficients for the 0° and 90° hollow cylinders. It is the 45° hollow cylinders that have large differences between the k- ω determined drag coefficients and the LES determined drag coefficients. The drag coefficients obtained using k- ω are consistently about 0.2 higher than the LES drag coefficients.

This difference is likely due to the way that the k- ω simulation models all turbulence while the LES resolves the larger scale turbulence. LES can more accurately model the turbulence that affects the value of the drag coefficient. This effect can be seen in the magnified velocity contours of Figure 24 and 25.

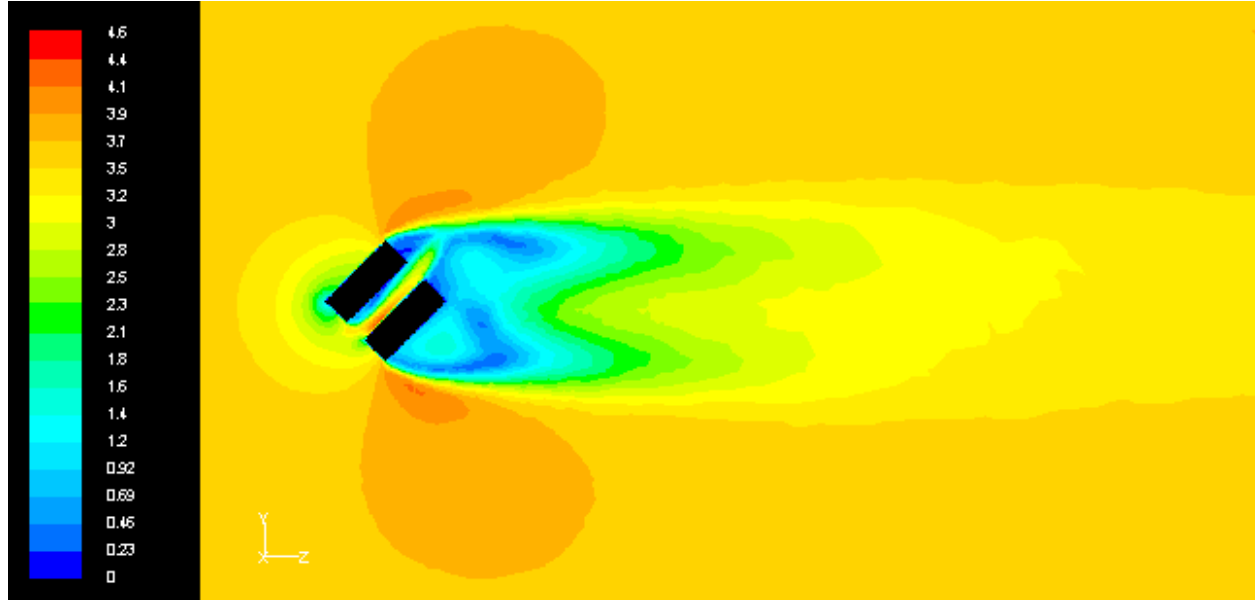


Figure 24. Velocity Contours (m/s), k- ω , 45° , Re=5000

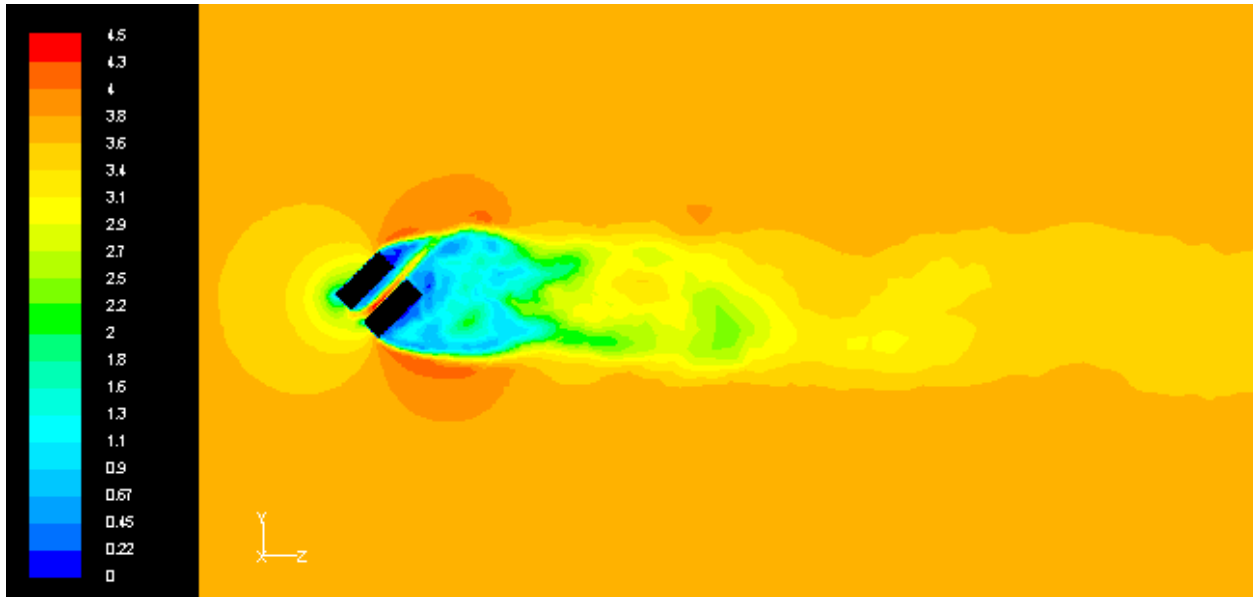


Figure 25. Velocity Contours (m/s), LES, 45°, Re=5000

Figure 24 and 25 show the effect that k- ω and LES have on modeling turbulence. Both have a similar overall structure. The k- ω has velocity contours that are more defined and symmetrical than the unsteady velocity contours given by LES however. LES features unsteady eddies in the flow trailing behind the cylinder.

The k- ω model is creating a larger wake behind the cylinder. The low velocity area behind the cylinder is what is responsible for the form drag on the hollow cylinder. The k- ω model seems to overestimate the size of the wake, which results in the larger drag coefficient.

Checking Domain and Mesh

It was important to ensure that the size of the mesh was sufficiently large so that the solution would not be affected by the walls surrounding the mesh. Increasing the mesh's dimensions should not affect the value of the drag coefficient obtained using it. Table 1 shows the % difference between the drag coefficient obtained in the original k- ω simulation and the drag coefficient obtained when using a larger domain size.

Table 1. Domain Percent Difference

| | 0° | 45° | 90° |
|----------|------------|----------|----------|
| Re=1000 | 3.31685393 | 9.796076 | 0.734742 |
| Re=5000 | 0.29225524 | 0.538461 | 2.485725 |
| Re=10000 | 6.98518591 | 0.207455 | 3.014758 |

The most significant error due to the domain size occurs with the 45° hollow cylinder at a Reynolds number equal to 5000. This is possibly due to the effect of the domain walls on the static pressure. Figure 26 show the static pressure contours for the entire domain of the original case of 45° angled

cylinder with Reynolds number equal to 1000.

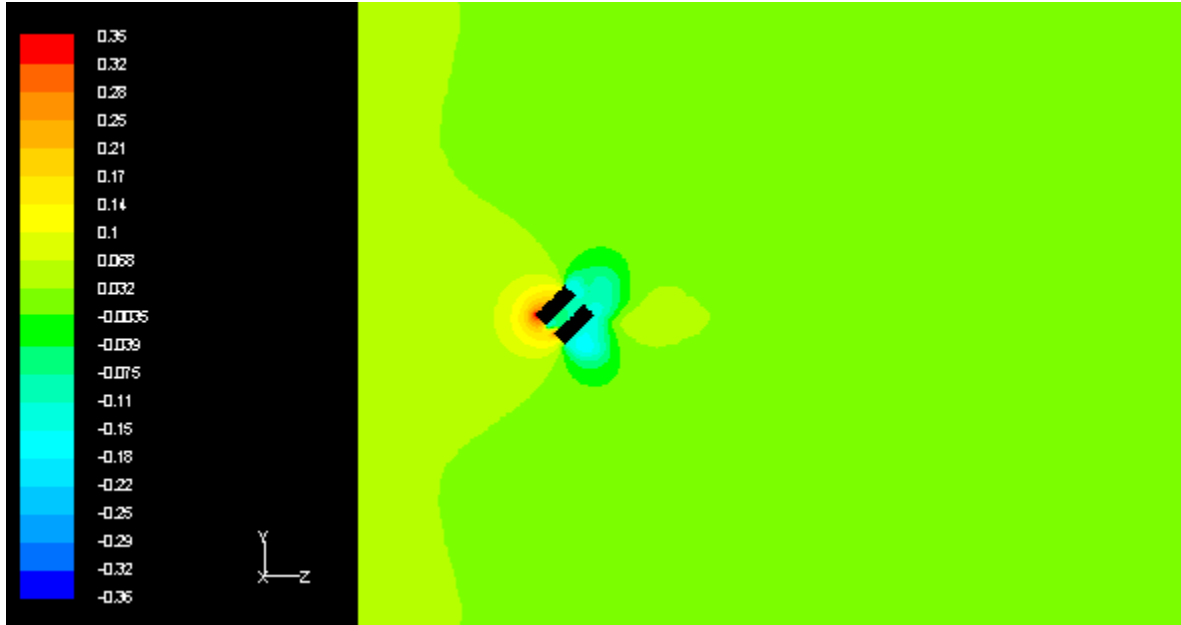


Figure 26. Static Pressure (Pa), k- ω , 45°, Re=1000

The static pressure around the cylinder could be affected by the proximity to the left boundary, causing an incorrect amount of drag force to be calculated. With the expanded domain the flow has longer to go before it reaches the cylinder, leaving plenty of room for the turbulence to not be affected by the outer walls of the domain.

It also was necessary to adapt the mesh to make sure that the original mesh could adequately handle the flow simulation. Table 2 shows the % difference between the drag coefficient obtained in the original k- ω simulation and the drag coefficient obtained after adapting the mesh once. The 90° mesh originally had 200390 nodes.

Table 2. Adapted 90° Mesh Difference

| | % error | final # of nodes |
|----------|----------|------------------|
| Re=1000 | 1.159945 | 256139 |
| Re=5000 | 0.265592 | 256017 |
| Re=10000 | 0.161586 | 255993 |

The potential error due to a poorly adapted mesh is not large enough to have a significant effect on the results. The solutions are grid independent.

Conclusion and Recommendations

The goal of this project was to compare the drag coefficient of a hollow cylinder at three different inclinations relative to fluid flow (0° , 45° , and 90°) and three different Reynolds numbers (1000, 5000, and 10000) obtained using RANS with the drag coefficient obtained using LES. Results were compared with values from the correlation developed by Hölzer & Sommerfeld (2008) and the solutions were tested to ensure solution independence. Validation of results was done by comparing CFD results for a sphere with experimental data on the drag coefficient of spheres.

From this came several conclusions. The SST k- ω model and the LES model both gave similar results for the hollow cylinder angled at 0° or 90° with respect to the main flow direction. For those angles it is recommended to use the SST k- ω model rather than the more computationally expensive LES.

For the 45° angled hollow cylinder using the SST k- ω model gave drag coefficient values that were about 0.2 higher than the drag coefficient values obtained using LES. Because of this it is recommended that LES be used when possible to determine the drag coefficient of hollow cylinders inclined at angles between 0° and 90° with respect to the main flow direction.

It was found that the 90° hollow cylinder could be treated like a 90° full cylinder for the purpose of determining the velocity profile and the drag coefficient.

The project findings could be expanded by experimentally determining the drag coefficient of a hollow cylinder at various angles and Reynolds numbers so that differences between the drag coefficients given by the correlation and the drag coefficients determined by CFD can be explained. Also, the effect of changes in the particle's shape could be studied. The usefulness of using LES or RANS for determining other heat or mass transfer coefficients could be studied.

References

- Afandizadeh, S., & Foumeny, E. A. (2001). Design of packed bed reactors: guides to catalyst shape, size, and loading selection. *Applied thermal engineering*, 21(6), 669-682.
- Chhabra, R. P., Agarwal, L., & Sinha, N. K. (1999). Drag on non-spherical particles: an evaluation of available methods. *Powder Technology*, 101(3), 288-295.
- Christiansen, E. B., & Barker, D. H. (1965). The effect of shape and density on the free settling of particles at high Reynolds numbers. *AIChE Journal*, 11(1), 145-151.
- Drag of a sphere*. (2010, September 16). Retrieved from <http://www.grc.nasa.gov/WWW/k-12/airplane/dragosphere.html>
- Ehrhard, J., Khatib, I. A., Winkler, C., Kunz, R., Moussiopoulos, N., & Ernst, G. (2000). The microscale model MIMO: development and assessment. *Journal of Wind Engineering and Industrial Aerodynamics*, 85(2), 163-176.
- Eigenberger, G., & Ruppel, W. (1997). Catalytic Fixed-Bed Reactors. *Ullmann's Encyclopedia of Industrial Chemistry*.
- Fluent Inc. (2006). FLUENT 6.3 User's Guide. Lebanon, New Hampshire, United States of America.
- Fröhlich, J., & von Terzi, D. (2008). Hybrid LES/RANS methods for the simulation of turbulent flows. *Progress in Aerospace Sciences*, 44(5), 349-377.
- Ganser, G. H. (1993). A rational approach to drag prediction of spherical and nonspherical particles. *Powder Technology*, 77(2), 143-152.
- Hoerner, S. (1958). *Fluid-dynamic drag; practical information on aerodynamic drag and hydrodynamic resistance*. (2 ed.). Midland Park, N.J.
- Hölzer, A., & Sommerfeld, M. (2008). New simple correlation formula for the drag coefficient of non-spherical particles. *Powder Technology*, 184(3), 361-365.
- Leith, D. (1987). Drag on nonspherical objects. *Aerosol science and technology*, 6(2), 153-161.
- Menter, F. R., Kuntz, M., & Langtry, R. (2003). Ten years of industrial experience with the SST turbulence model. *Turbulence, heat and mass transfer*, 4, 625-632.
- Michaelides, E. (2006). *Particles, bubbles & drops: their motion, heat and mass transfer*. (p. 171). Singapore: World Scientific.
- Preukschat, A. W. (1962). *Measurements of Drag Coefficients* (Doctoral dissertation, California Institute of Technology).

Priyadarshini, V. (2012). *Study of Drag Coefficient Using CFD Tools* (Doctoral dissertation, National Institute of Technology Rourkela).

Roos, F., & Willmarth, W. (1971). Some experimental results on sphere and disk drag. *AIAA Journal*, 9(2), 285-291.

Salim, S. M., Ong, K. C., & Cheah, S. C. (2011). Comparison of RANS, URANS and LES in the prediction of airflow and pollutant dispersion. In *Proceedings of the World Congress on Engineering and Computer Science* (Vol. 2).

Stitt, E. (2005). *Substainable strategies for the upgrading of natural gas*. NATO Science Series II Mathematics, Physics, & Chemistry , 191, 185-216.

Tran-Cong, S., Gay, M., & Michaelides, E. E. (2004). Drag coefficients of irregularly shaped particles. *Powder Technology*, 139(1), 21-32.

U.S. Climate Change Technology Program, (2005). *Technology options for the near and long term*. Retrieved from website: <http://www.climatechange.gov/library/2005/tech-options/tor2005-143.pdf>